Tracing Clonal Dynamics Reveals that Two- and Three-dimensional Patient-derived Cell Models Capture Tumor Heterogeneity of Clear Cell Renal Cell Carcinoma

Journal Article

Author(s):
Bolck, Hella A.; Corrò, Claudia; Kahraman, Abdullah; von Teichman, Adriana; Toussaint, Nora C.; Kuipers, Jack; Chiovaro, Francesca; Koelzer, Viktor H.; Pauli, Chantal; Moritz, Wolfgang; Bode, Peter K.; Rechsteiner, Markus; Beerenwinkel, Niko (iD); Schraml, Peter; Moch, Holger

Kidney Cancer

Tracing Clonal Dynamics Reveals that Two- and Three-dimensional Patient-derived Cell Models Capture Tumor Heterogeneity of Clear Cell Renal Cell Carcinoma

Hella A. Bolck [a,†], Claudia Corrò [a,†], Abdullah Kahraman [a], Adriana von Teichman [a], Nora C. Toussaint [b,c], Jack Kuipers [c,d], Francesca Chiovaro [e], Viktor H. Koelzer [a], Chantal Pauli [a], Wolfgang Moritz [e], Peter K. Bode [a], Markus Rechsteiner [a], Niko Beerenwinkel [c,d], Peter Schraml [a,*,‡], Holger Moch [a,‡]

[a] Department of Pathology and Molecular Pathology, University Hospital and University of Zurich, Zurich, Switzerland; [b] NEXUS Personalized Health Technologies, ETH Zurich, Zurich, Switzerland; [c] SIB Swiss Institute of Bioinformatics, Basel, Switzerland; [d] Department of Biosystems Science and Engineering, ETH Zurich, Basel, Switzerland; [e] InSphero AG, Schlieren, Switzerland

Article info

Abstract

Background: Extensive DNA sequencing has led to an unprecedented view of the diversity of individual genomes and their evolution among patients with clear cell renal cell carcinoma (ccRCC).
Objective: To understand subclonal architecture and dynamics of patient-derived two-dimensional (2D) and three-dimensional (3D) ccRCC models *in vitro*, in order to determine whether they mirror ccRCC inter- and intratumor heterogeneity.
Design, setting, and participants: We have established a comprehensive platform of living renal cancer cell models from ccRCC surgical specimens.
Outcome measurements and statistical analysis: We confirmed the concordance of 2D and 3D patient-derived cell (PDC) models with the original tumor tissue in terms of histology, biomarker expression, cancer driver mutations, and copy number alterations. We addressed inter- and intrapatient heterogeneity by analyzing clonal dynamics during serial passaging.
Results and limitations: In-depth genetic characterization verified the presence of heterogeneous cell populations, and revealed a high degree of similarity between subclonal compositions of monolayer and organoid cell cultures and the corresponding parental ccRCCs. Clonal dynamics were evident during serial passaging of cells *in vitro*, suggesting that PDC cultures can offer insights into evolutionary potential and treatment susceptibility of ccRCC subclones *in vivo*. Proof-of-concept drug profiling using selected ccRCC-targeted therapy agents highlighted patient-specific vulnerabilities in PDC models that could not be anticipated by interrogating commercially available cell lines.
Conclusions: We demonstrate that PDC models mirror inter- and intratumor heterogeneity of ccRCC in vitro. Based on our findings, we envision that the use of these models will advance our understanding of the trajectories that cause genetic diversity and their consequences for treatment on an individual level.
Patient summary: In this study, we developed two- and three-dimensional patient-derived models from clear cell renal cell carcinoma (ccRCC) as "mini-tumors in a dish." We show that these cell models retain important features of the human ccRCCs such as the profound tumor heterogeneity, thus highlighting their importance for cancer research and precision medicine.

† These authors contributed equally to this work.
‡ These authors share senior authorship.
* Corresponding author. Department of Pathology and Molecular Pathology, University Hospital Zurich, Schmelzbergstrasse 12, 8091 Zurich, Switzerland. Tel.: +41 (0)44 2552537.
E-mail address: Peter.Schraml@usz.ch (P. Schraml).

1.   Introduction

Kidney cancers are a heterogeneous group of chemotherapy-resistant diseases associated with very high mortality [1]. The most frequent subtype is clear cell renal cell carcinoma (ccRCC) that is characterized by specific histopathological features and an almost universal loss of chromosome 3p often concurrent with gain of chromosome 5q [2–4]. This translocation is considered to produce a small number of tumor-initiating cells early in life, which over time acquire the necessary additional genetic alterations, such as inactivation of the remaining chromosome 3p-encoded *VHL* tumor suppressor. These alterations eventually trigger clinically relevant ccRCC most often in the 7th decade of life [4,5].

Clear cell RCC is characterized by high levels of intra- and intertumor heterogeneity that arises from clonal expansion and parallel evolution driven by the initiating genetic events [4,6–8]. Recently, extensive multiregional genetic sequencing has suggested that at least seven distinct evolutionary patterns of ccRCC tumorigenesis exist that correlate with clinical phenotypes and contribute to patient outcome [8]. However, profiling of intra-tumor genetic heterogeneity has not been integrated into therapeutic decision making and clinical management of ccRCC patients to date. Targeted therapies developed based on the common molecular underpinning of ccRCCs have improved patient outcomes only moderately [1,9], and it is plausible that marked inter- and intratumor heterogeneity of ccRCCs has hampered their benefit. As tumor cell heterogeneity adds a new level of complexity to the molecular basis of ccRCC, preclinical models that can mirror this feature *in vitro* would be an attractive approach to advance the understanding of ccRCC tumor biology and identify new therapeutic options. However, the most widely used human-derived *in vitro* models to date are monoclonal cell lines that often fail to capture the genetic complexity of ccRCC [10–13].

We have established a comprehensive platform of well-characterized living renal cancer cells. These preclinical cancer models require no xenografting or exogenous gene transfer, and are therefore closely related to the human tumor. We provide a thorough phenotypical and molecular analysis of two- and three-dimensional (2D and 3D) patient-derived cell (PDC) models, verifying their concordance with the corresponding patient tumors and their capability of reflecting ccRCC inter- and intrapatient genetic heterogeneity. Moreover, we explore the feasibility of drug testing on different PDC models in order to demonstrate that ccRCC-derived cell cultures constitute a new generation of *in vitro* tools that will expand our understanding of how inter- and intratumor heterogeneity affects patient outcomes.

2.   Patients and methods

A detailed description of the patients and methods is available in the Supplementary material.

2.1.   Ethics statement

All tissue samples were made available by the Tissue Biobank of the Department of Pathology and Molecular Pathology, University Hospital of Zurich, Switzerland. The local ethics commission approved this study (KEK-ZH-Nr. 2011-0072 and KEK-ZH-Nr. 2014-0614), and all patients gave written consent.

3.   Results

3.1.   Establishing a living biobank of PDCs from ccRCCs

In order to develop adequate *in vitro* models of ccRCC, we have extended routine tumor tissue biobanking with a repository of patient-derived living cells from human tumors (Fig. 1A). We obtained surplus tissue from patients, who underwent ccRCC resection, subsequent to a pathological review. Over a period of 3 yr, we acquired 35 specimens (Supplementary Table 1). Targeted sequencing of the *VHL* gene revealed that 80% of tumors from this cohort (28/35) harbored a somatic mutation of at least one allele (Supplementary Table 1). In 74% of the cases (26/35), we successfully established monolayer PDC cultures and expanded them for at least three passages (Fig. 1B and Supplementary Table 1; patients 1–26). Doubling times of PDC monolayer cultures were generally variable, and usually ranged between 5 d and 4 wk. Importantly, the PDC cultures generated here were not immortalized, and the growth conditions that we used stimulated proliferation for a limited amount of time. Often PDCs underwent senescence after five to ten passages. To facilitate biobanking, we cryopreserved dissociated tumor cells and validated cells from early passages, which will continue to proliferate upon thawing.

VHL sequencing in the cell cultures at various passage numbers demonstrated that 74% of samples (14/20) displayed the same *VHL* mutation as the primary tumor (Fig. 1B). Within the detection limit of Sanger sequencing [14], six PDC cultures failed to exhibit the *VHL* mutation of the original ccRCCs, indicating that nontumor cells might have prevailed during in vitro cell growth. In the six remaining ccRCCs with VHL wild-type mutational status (Supplementary Table 1; patients 1, 14, 16, 20, 22, and 26), cytogenetic aberrations of chromosome 3 were analyzed and found to be matching between parental ccRCCs and corresponding cell cultures (Supplementary Fig. 1A and 1B). Consequently, we could verify that the genotypic alterations of the primary tumor were matched by 77% (20/26) of cell cultures.

In addition, we assessed possible reasons for the failure of culture derivation in the nine ccRCCs from which no PDC models could be generated (Supplementary Table 1; patients 27–35). Genetic and protein expression features were indistinguishable between tumors from which PDC cultures could be established and those from which it failed. On the phenotypic and morphological level, we observed that tumors of low grade and displaying high levels of necrosis showed an increased likelihood of failing in cell culture derivation (Supplementary Table 1 and Supplementary Fig. 2C).
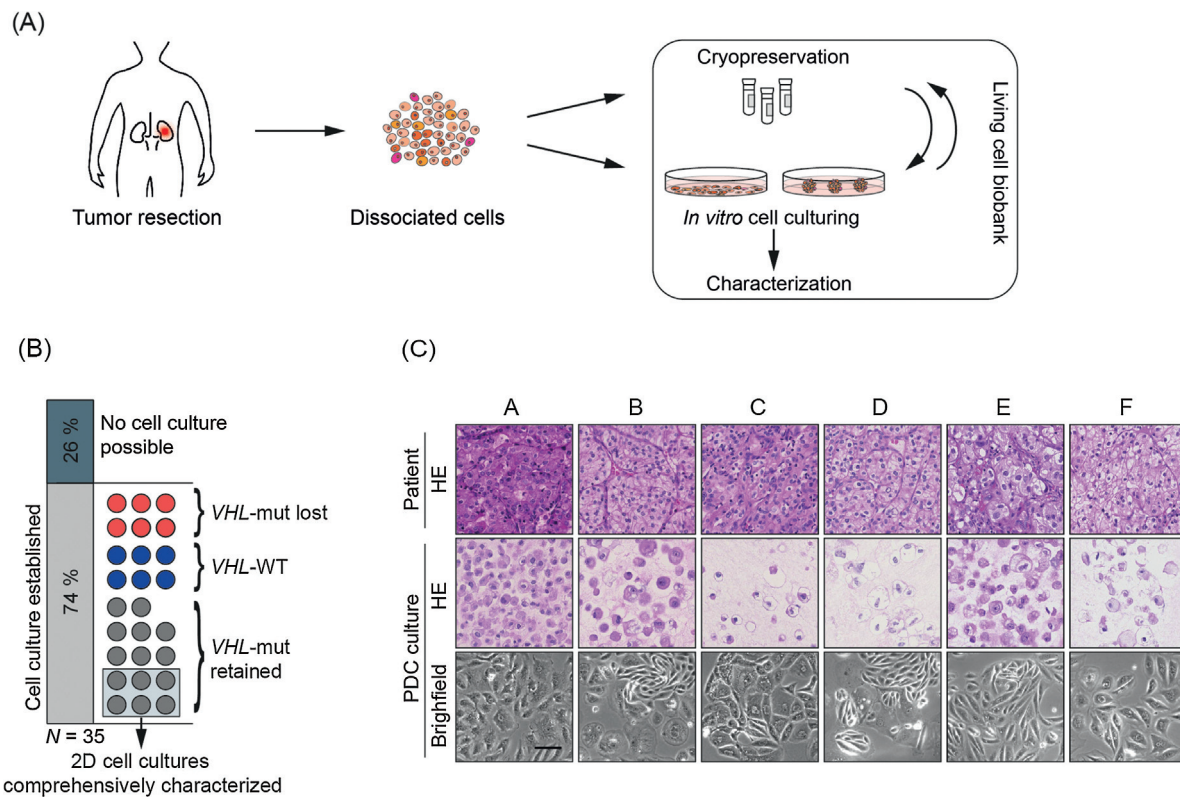
Fig. 1 – Establishing a living biobank for ccRCC-derived cell models. (A) Diagram depicting the generation of PDC models from ccRCC surgical specimens. Fresh tumor tissue is processed into dissociated single cells that are subsequently used to establish two- and three-dimensional (2D and 3D) cell models or cryopreserved for later use. In addition, established cell cultures are frequently viably frozen for biobanking purposes. **(B)** Bar chart of ccRCC surgical specimens that have been considered for the generation of PDC cultures over 3 yr. Cell culture derivation was not possible if no viable cells remained following tissue processing or cells did not proliferate sufficiently in culture. Successfully established cell cultures could be expanded for at least three passages. In these cases, primary ccRCCs and corresponding cell cultures were subjected to *VHL* mutation profiling, and the number of PDC cultures retaining the *VHL* mutation of the original tumor is indicated. *VHL*-WT tumors and corresponding cell cultures were further analyzed by FISH of chromosome 3 (refer to Supplementary Fig. 1). Six representative ccRCC-derived cell cultures were comprehensively characterized. **(C)** HE images of primary tumors (FFPE) and corresponding FFPE cytoblocks from PDC cultures for histological evaluation (20× objective). Light microscope images of the same PDC cultures depict morphology during 2D cell growth (10× objective). Scale bar denotes 50 μm. ccRCC = clear cell renal cell carcinoma; FFPE = formalin-fixed paraffin embedded; FISH = fluorescence in situ hybridization; HE = hematoxylin eosin; PDC = patient-derived cell; WT = wild type.

In order to evaluate whether patient-derived renal cell models reflect important aspects of ccRCC tumor biology such as the strong tumor heterogeneity, we next sought to profile six representative patient cases and corresponding *in vitro* cell models by analyzing histology, biomarker expression, copy number variations, drug responses, and somatic mutations. Importantly, all the six primary ccRCCs harbored mutations in the *VHL* gene (Table 1).

3.2. Histological, molecular and functional characterization of ccRCC *in vitro* models

Selected patient-derived monolayer cultures displayed typical epithelial features, but individual cell cultures differed in their morphology (Fig. 1C and Supplementary Fig. 1C). PDC cultures recapitulated hallmarks of ccRCC histology such as enlarged pleomorphic nuclei and conspicuous eosinophilic nucleoli. Since prominent nucleoli determine ccRCC tumor grade, we sought to quantify this parameter in order to provide an unambiguous comparison between the original tumors and PDC cultures (Supplementary Fig. 1C).

Importantly, we found that nucleoli sizes correlated with ccRCC tumor grades. Overall, the nucleolar perimeters that we measured in PDC cultures were in good agreement with those of the corresponding parental ccRCCs (Supplementary Fig. 1C). However, slight variation was evident, particularly for the PDC cultures derived from patients A, B, and C. We perceive that this variability could be due to different levels of cellular changes that occurred during sample processing of formalin-fixed paraffin-embedded (FFPE) cytoblocks. In support of this hypothesis, we observed higher levels of hydropic degeneration and membrane rupture in the hematoxylin eosin–stained section of these specimens (Fig. 1C). We also segmented nuclear features and recorded shape parameters such as area, perimeter, and eccentricity. These showed good agreement between FFPE specimens of the original ccRCCs and corresponding cell cultures, indicating that morphological parameters were largely preserved during cell culture (Supplementary Fig. 1C).

Additionally, expression of the most prevalent biomarkers generally agreed between PDC cultures and original ccRCCs. All PDC cultures retained Pax8 and pan-cytokeratin

Table 1 – Summary of clinical data and patient characteristics of six representative ccRCC cases that were comprehensively studied.

Internal #	Age	Gender	Disease status at cell culture derivation	Organ from which cell culture was derived	Metastasis	Tumor diameter (cm)	Grade (WHO/ISUP)	Stage	VHL mutation	Adjuvant therapy received	Therapeutic agent	Patient Outcome
A	68	M	Primary	Adrenal gland	Yes	1.6	3	pT3a	c.IVS1-1G > C/(c.341-1G > C)	NA	NA	Recurrent disease
B	70	M	Primary	Kidney	No	5	2	pT3a	c.158_164del/p.Glu53GlyfsX12	No	NA	Disease-free survival
C	71	M	Primary	Kidney	No	5.6	2	pT1b	c.533_537del/p.Leu178HisfsX76	No	NA	Disease-free survival
D	49	M	Primary	Kidney	No	9.5	3	pT3a	c.579insA/p.Asp193LysfsX63	No	NA	Disease-free survival
E	53	M	Primary	Kidney	Yes	12	4	pT3a	c.74C > T/p.Pro25Leu	Yes	Pazopanib	Death from disease
F	75	F	Recurrent	Kidney	Yes	4	2	rpT3a	c.IVS1 + 1G > A (c.340 + 1G > A)	No	NA	Recurrent disease

ccRCC = clear cell renal cell carcinoma; ISUP = International Society for Urological Pathology; NA = not available; WHO - World Health Organization.

expression, validating their renal epithelial origin. Similarly, all but one PDC culture showed expression of the classical ccRCC-specific markers CAIX and CD10 (Fig. 2A and B, and Supplementary Fig. 3A–E). Interestingly, two commercially available ccRCC cell lines (Caki1 and 769 P) did not express either CAIX or CD10 (Supplementary Fig. 3F).

Genome-wide copy number analysis revealed the presence of the most common CNAs, loss of chromosome 3p often concurrent with gain of chromosome 5q, in all primary ccRCCs of this cohort (Fig. 2C and Supplementary Fig. 4) [4]. PDC cultures retained large-scale CNAs throughout their genomes with the exception of patient E, for whom the loss of chromosome 3p appeared to be subclonal in the tumor and was not captured by the PDCs (Supplementary Fig. 4). Interestingly, the majority of cell cultures showed cleaner and more distinct CNA signals than original ccRCCs, probably due to the selection of dominant subclones during serial passaging. For example, a subpopulation of cells with chromosome 7 amplification became more pronounced in the culture derived from patient A, while subpopulations with chromosome 8 amplification and chromosome 14 deletions were hardly retained during serial passaging of the cell culture from patient C.

To functionally analyze a subset of PDC cultures and compare them with commercially available ccRCC cell lines, we performed drug profiling with sunitinib, everolimus, and cabozantinib, used for first-, second-, and third-line treatment of ccRCC, respectively [15] (Fig. 2D and 2 E). Not unexpectedly, PDC cultures and commercially available cell lines displayed distinct drug sensitivity profiles (Fig. 2E). Strikingly, we observed substantial differences in the responses of PDC cultures and commercially available cell lines, particularly toward cabozantinib and everolimus. Caki1 and 769 P cells were almost resistant to cabozantinib, an inhibitor of the VEGF, MET, and AXL receptors [16]. In contrast, PDC cultures displayed distinct sensitivities toward this agent, which may be reflective of recent findings presenting it as the most efficacious newly developed tyrosine kinase inhibitor *in vivo* [17]. The two cell lines were most susceptible to the mTOR inhibitor everolimus, which was not matched by the PDC cultures. From our cohort, only patient E received adjuvant treatment with pazopanib subsequent to nephrectomy but exhibited tumor progression under this therapy. Remarkably, cells derived from this tumor showed only moderate sensitivity to pazopanib *in vitro* (Supplementary Fig. 4G).

3.3. Characterization of patient-specific genetic alterations in ccRCCs and PDC cultures

In order to define the landscape of genetic alterations in the six ccRCCs and corresponding PDC cultures, next-generation sequencing of 409 cancer-related genes was performed. Overall, genotypes were concordant across patient-matched normal and tumor tissue as well as corresponding PDC cultures. Indeed, patient-specific DNA samples clustered together, but signatures differed significantly between patients (Fig. 3A). The total number of nonsynonymous
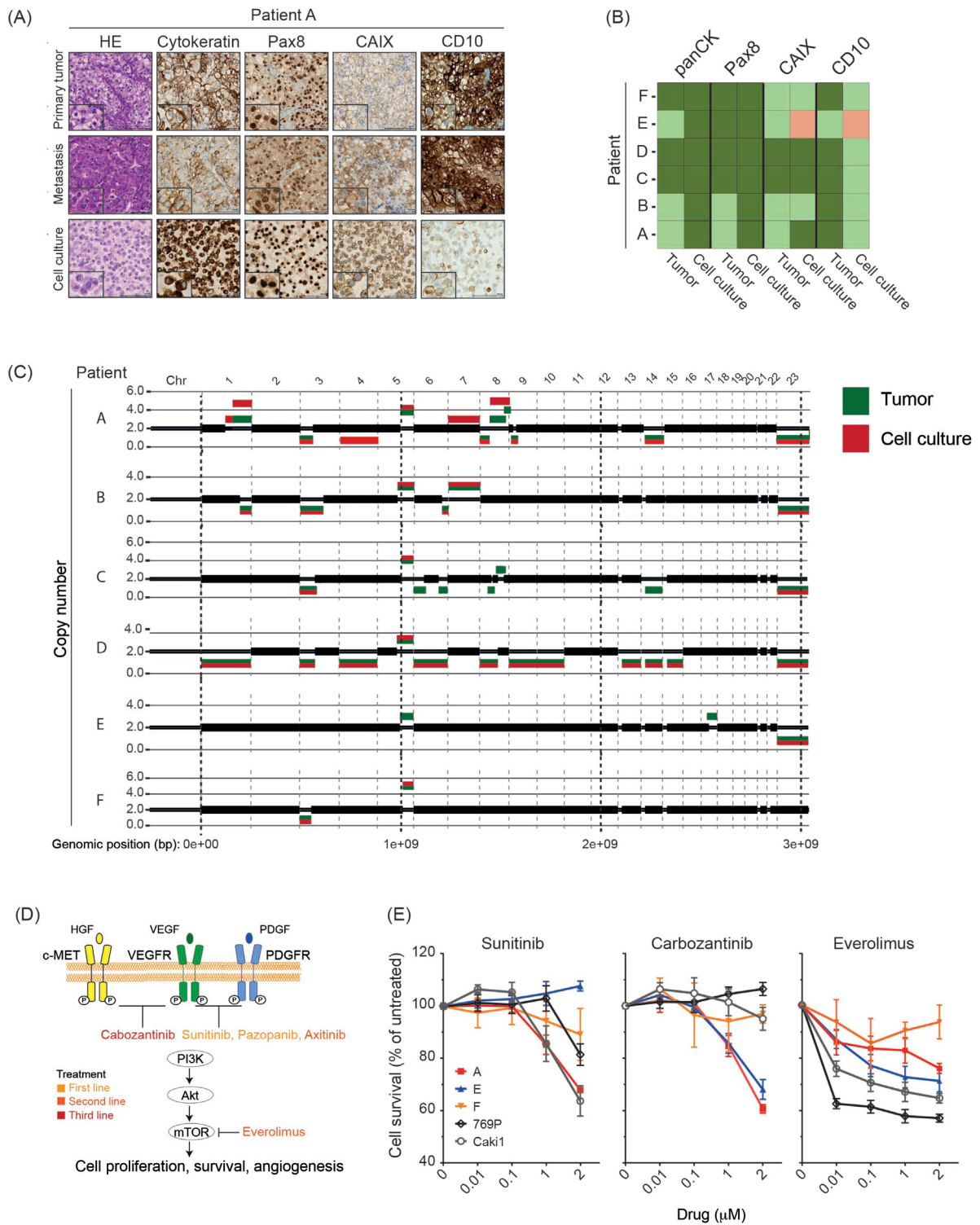
Fig. 2 – Molecular and functional characterization of ccRCC-derived monolayer cultures. (A) Histopathological analysis of FFPE primary tumor, metastasis of the adrenal gland, and corresponding FFPE cytoblock from the PDC culture derived of the metastasis (20× objective, insets 40× objective). Consecutive sections were stained with HE or the indicated antibodies by IHC. Scale bars denotes 100 μm. (B) Summary of biomarker expression in original ccRCC tumors or metastasis and corresponding PDC cultures as illustrated for patients A–F (Fig. 3A, left side). Representative images are shown in Supplementary Fig. 2. (C) Genome-wide CNAs of parental ccRCCs and matched PDC cultures. CNAs were derived from CytoScan HD array. Y axis depicts estimated copy numbers after data normalization on the neutral two-copy level. Green color represents copy number gains and deletions of the primary ccRCCs, and red color represents the corresponding PDC culture. Genomic profiles indicating Log2 ratios of all samples are shown in Supplementary Fig. 3. (D) Simplified scheme of the AKT/mTOR signaling pathway including targeted drugs used in ccRCC treatment. (E) Dose-response curves for selected drugs from Fig. 2D. Cryopreserved cells were thawed, seeded into monolayer cultures for recovery, and subjected to drug profiling with increasing concentrations of the indicated drugs for 6 d. Cell viability of ccRCC patient–derived cell cultures or commercially available cell lines (769 P and Caki1) in the presence of selected drugs in vitro was assessed. $N \geq 3$, data are presented as mean ± SEM. ccRCC = clear cell renal cell carcinoma; CNA = copy number aberration; FFPE = formalin-fixed paraffin embedded; HE = hematoxylin eosin; IHC = immunohistochemistry; PDC = patient-derived cell; SEM = standard error of the mean; VEGF = vascular endothelial growth factor; VEGFR = vascular endothelial growth factor receptor.
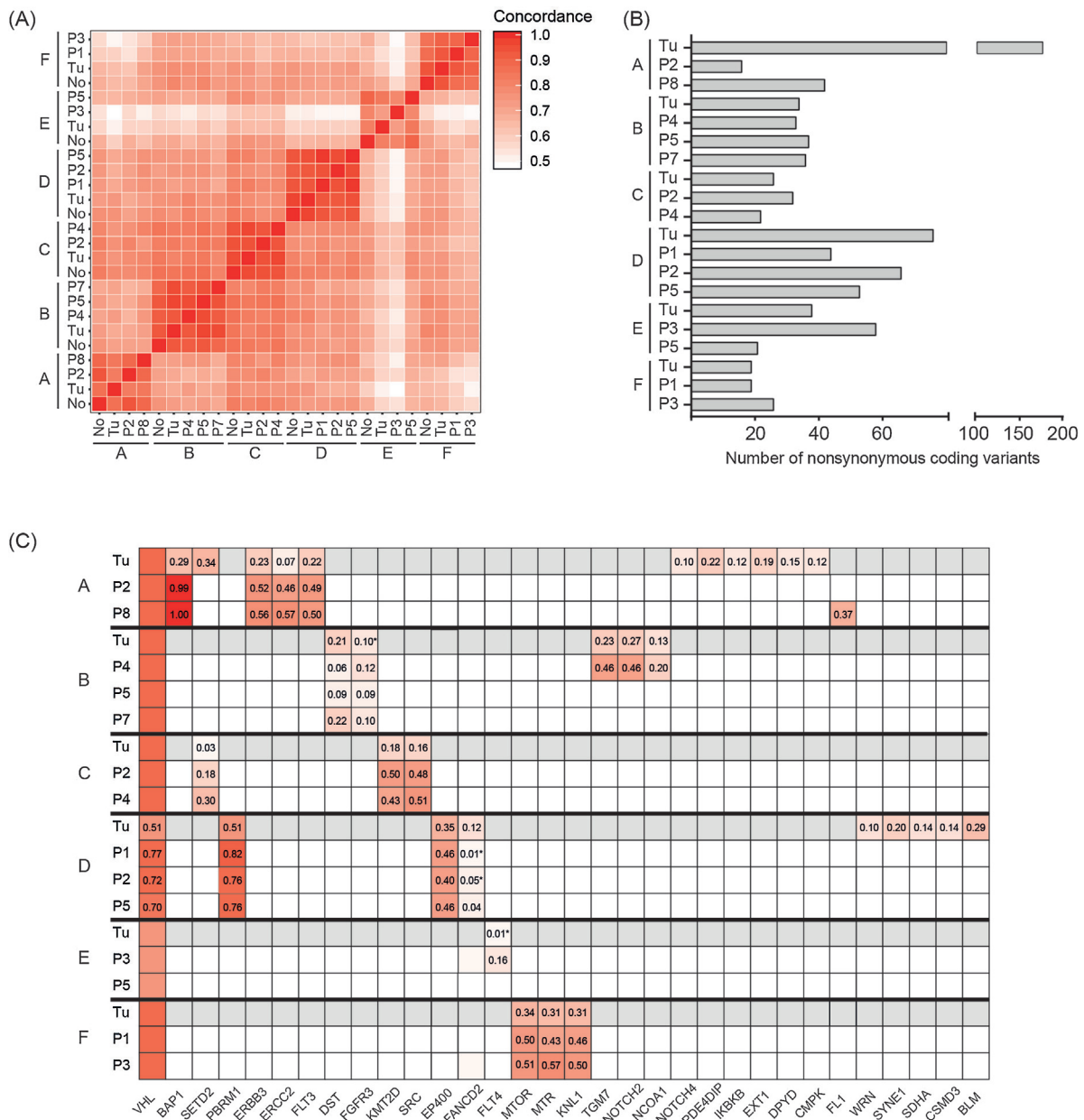
Fig. 3 – Analysis of cancer gene alterations in ccRCCs and corresponding PDC cultures. (A) Heatmap showing concordance between patient tissue and corresponding ccRCC-derived cell cultures determined based on a subset of loci, for which at least two different genotypes could be observed across all samples. Concordance scores are indicated by the color scale. (B) Bar graphs showing the total number of nonsynonymous coding variants (mutation load) per sample detected by next-generation sequencing of 409 cancer-related genes in patient tissue and corresponding ccRCC-derived cell cultures at the indicated passage numbers. (C) High-confidence, nonsilent somatic variants identified by NGS in DNA extracted from primary tumor (FFPE tissue—patients A and D, or dissociated primary cells of the original ccRCC—patients B, C, E, and F) and cultured cells at the designated passage numbers. VAFs are indicated and correspond to the color scale. VAFs marked with an asterisk were identified by manual inspection only as they failed to be reported during variant calling. ccRCC = clear cell renal cell carcinoma; FFPE = formalin-fixed paraffin embedded; NGS = next-generation sequencing; PDC = patient-derived cell; VAF = variant allele frequency.

coding variants was generally stable during cell culture derivation and propagation (Fig. 3B), indicating that genetic changes due to cell culture techniques were minimal.

Besides the *VHL* driver mutations, the six original ccRCCs and corresponding PDC cultures were affected by nonsynonymous alterations in relevant ccRCC genes, such as *PBRM1*, *SETD2*, and *BAP1,* as well as by a number of additional somatic changes. Importantly, mutations were consistent between primary tumor and the corresponding

cell cultures, and largely specific to individual patients reflective of interpatient genetic heterogeneity (Fig. 3C). Allele frequencies often increased during serial passaging of PDC cultures, suggesting that certain genetic changes may confer growth advantages *in vitro*. A subset of mutations with low or moderate frequencies was observed only in the primary tumor, particularly of patients A and D, and could not be continuously detected in the corresponding cell cultures. The loss of tumor-specific

variants during cell culturing appeared to be lower when DNA from PDCs was compared with DNA from fresh primary tumor cells (Fig. 3C; patients B and C). When DNA obtained from FFPE tumor tissue was used as a reference (Fig. 3C; patients A and D–F), the number of mutations that could not be detected in the associated cell cultures increased, suggesting the presence of sampling discrepancies or formalin-induced sequencing artifacts [18]. Accumulation and loss of mutations during serial passaging resulted in more distinct genomic signatures in PDC cultures over time, and also suggested that certain subclones may have prevailed in culture while others have diminished.

3.4. Clonal dynamics and retention of intratumor heterogeneity in ccRCC PDC cultures

Given that recent studies have described profound genetic intratumor heterogeneity in sporadic ccRCC [4,6,8], we examined whether the subclonal architecture of parental ccRCCs was mirrored in their PDC cultures. To assess dynamics of cancer subpopulations, we applied the tumor phylogeny reconstruction algorithm PhyloWGS to the sequencing data of ccRCC samples and corresponding PDC culture passages [19]. Our analysis revealed that all PDC cultures were composed of genetically diverse subclonal populations of cells (Fig. 4A–F). The large majority of
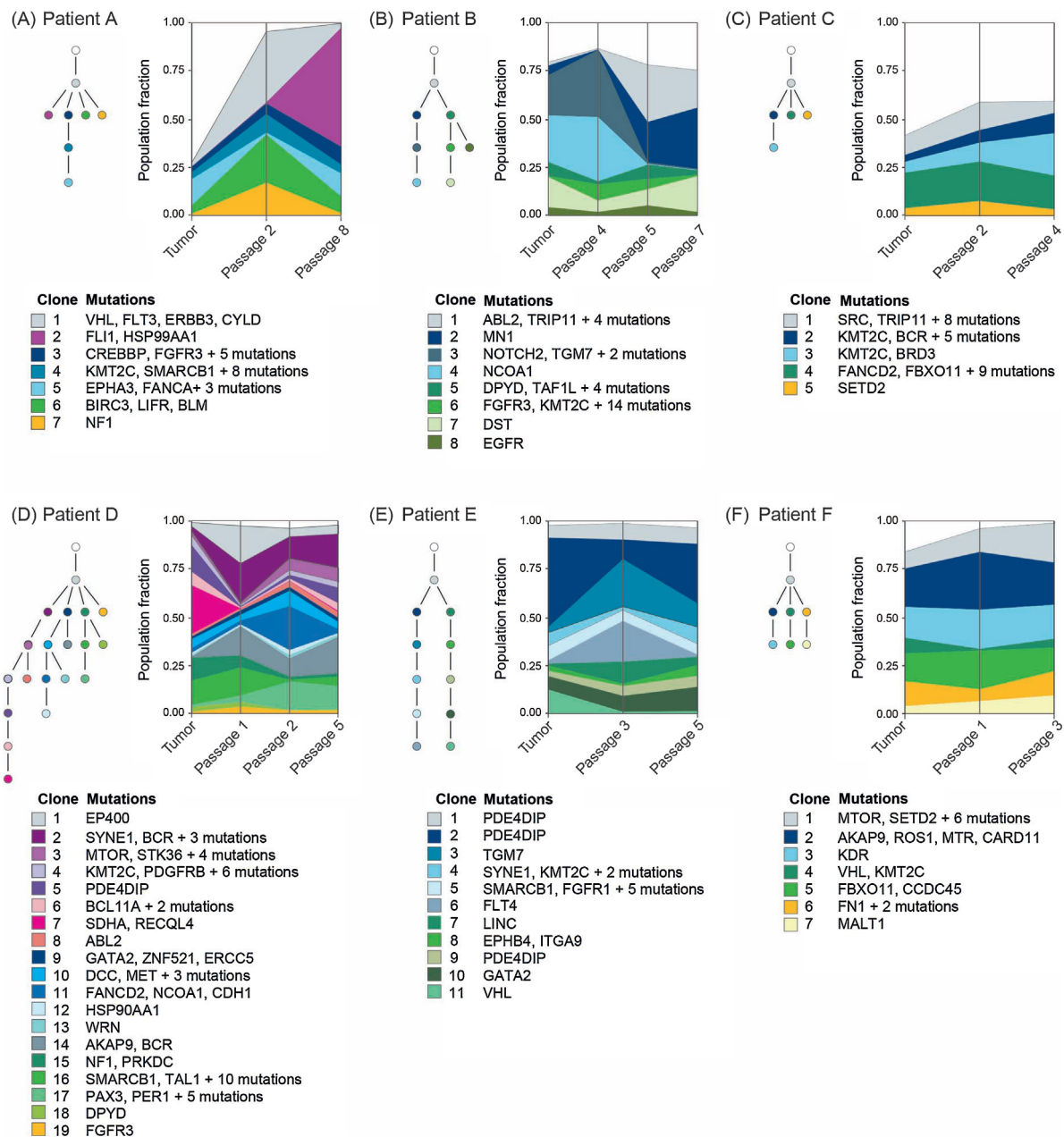
Fig. 4 – Clonal dynamics over multiple passages during PDC culturing. (A–F) Plots display clonal structure, and dynamics of the original tumors and subsequent PDC culture passages for patient samples A–F. Mutation clusters and relative prevalence were inferred by PhyloWGS from bulk population-level targeted sequencing data. Mutation tree reconstruction allowed the assessment of mutational histories and relationships between subclones. Variants defining a new node are indicated, and a more detailed list can be found in Supplementary Table 3. PDC = patient-derived cell.

clones observed in the PDC cultures could be traced back to the matched patient tumor tissue. Based on population frequencies of mutations that distinguished subclonal populations, PhyloWGS was used to infer trees depicting evolutionary relationships among distinct subpopulations of cells. This analysis revealed that the subclones of each ccRCC shared a common ancestor harboring a truncal set of driver mutations. Additional accumulation of genetic variants resulted in branched evolution of subsequent clones, which contained variants in both coding and noncoding regions of the genome (Supplementary Table 3). The clonal composition of PDC cultures was in general relatively stable with increasing passage numbers. However, we also observed dynamic behavior in subclonal architectures, for instance, during *in vitro* clonal evolution of the PDC culture of patient B, clones 3 and 4 were lost after passage 5. This was consistent with the observation that a small number of somatic coding variants were not retained during PDC propagation, such as the NOTCH2, TGM7, and NCOA1 variants that defined clones 3 and 4 in patient B (Fig. 4B and 3C). Although these two subclones expanded initially, they were later replaced by the ancestral clones 1 and 2 that are characterized by a different set of mutations (Supplementary Table 3). Frequently, we observed minor subclones of the original tumor undergoing significant expansion during in vitro culturing. Interestingly, many of the mutations contained in dominant subclones included alterations in known ccRCC drivers such as SETD2, PBRM1, KMT2C, FGFR3, and MTOR [8]. For instance, an early clone of the tumor of patient F that contained MTOR and SETD2 mutations (clone 1) expanded to being almost fully clonal by the time the corresponding PDC culture reached passage 3 (Fig. 4F and Supplementary Table 3). Changes in the prevalence of different clones were most substantial in patient A for which the branch originating from clone 3 (Fig. 4A, blue branch) was stable over time, while the early clone 1 was replaced by clone 2 that co-occurred with clones 6 and 7 (Fig. 4A). Although dynamic clonal behavior was observed in a subset of PDC cultures (patients A, B, and D), our analysis showed that for other cultures, such as those derived from patients C, E, and F, the clonal composition was remarkably stable over time. It is therefore perceivable that differences in clonal dynamics observed in PDC culture may mirror the possibility of parallel evolution of subclones that give rise to different levels of intratumor heterogeneity in vivo [8,20]. In summary, our data indicate that subclonal architecture was highly similar between parental ccRCCs and matched PDC cultures over several passages.

3.5. Generation of next-generation 3D cancer models and proof-of-principle analysis of drug responses

Owing to the limited capacity to accurately model the spatial complexity of human tumors and their microenvironment, monolayer cell cultures are often considered an oversimplified cell model. Recently developed 3D culture technologies promise to resemble and recapitulate the *in vivo* tissue environment more accurately [21,22]. In order to explore 3D cell culture models using patient-derived ccRCC cells, we thawed cryopreserved specimens to generate tumor organoids and microtissues. Tumor organoids were established as previously described [23], and could be generated from cryopreserved dissociated primary and passaged cells. It is important to note that in contrast to previously published protocols [23,24], ccRCC-derived organoids had to be cultivated in the absence of inhibitors of the Rho-associated coiled coil containing protein kinase (ROCK), as these impaired cell proliferation due to the synthetic lethal relationship with *VHL* deficiency [25]. Initial validation of the organoids was achieved by cytology that ensured the presence of cells with typical features of malignancy such as multiple pleomorphic nuclei and large nucleoli (Fig. 5A) [24,26]. Cytological assessment as well as gross morphology of organoids revealed the presence of different cell populations within one organoid line possibly representing distinct subclonal entities. Subclonal composition of the organoid lines was further corroborated by genomic profiling and analysis of clonality with PhyloWGS. Importantly, nonsilent somatic coding variants were mostly consistent between the original ccRCCs and corresponding organoid cultures, and similarly to monolayer PDC cultures, patient-specific mutational signatures were maintained *in vitro* (Fig. 5B). Pre-existing subclones of the original ccRCCs were largely present in the corresponding organoid cultures (Fig. 5C). However, compared with monolayer PDC cultures, we noted partially different patterns of selection and expansion of branched subclones. Particularly in the organoid line derived from patient E, we observed a relative increase of subpopulations originating from clone 7 (right branch), which contained sets of mutations not present in the corresponding monolayer PDC culture (Fig. 4E). This effect was less striking in the organoids derived from patient A, for which the subclonal population that resembled and differed from those detected in the monolayer PDC cultures seemed to coexist during organoid culture (Fig. 4A). Taken together this indicated that clonal dynamics at least partly depend on cell culture conditions, and further studies are required to interpret the diversity observed between different techniques.

Likewise, dissociated primary as well as passaged frozen cells aggregated into microtissues of about 100–200 μm in diameter within 3 d under the condition that exogenous fibroblasts (normal human dermal fibroblasts [nHDFs]) were supplied at a ratio of at least 1:20. However, cell models validation by immunohistochemistry revealed that important ccRCC biomarkers were not reliably retained as the prevalence of the stromal component likely presented a significant problem (Supplementary Fig. 5A). Moreover, the addition of nHDFs masked tumor cell–specific mutations and thus impeded genetic analysis of these cell models.

Organoids and microtissues derived from patient A were used for a proof-of-principle drug response assay to investigate whether the effects from monolayer cell models could be replicated (Supplementary Fig. 5B). Owing to their nonuniform sizes and morphological heterogeneity in microplate wells, drug screening of the organoid culture posed substantial technical challenges and resulted in larger variability between replicates. Microtissues, on the
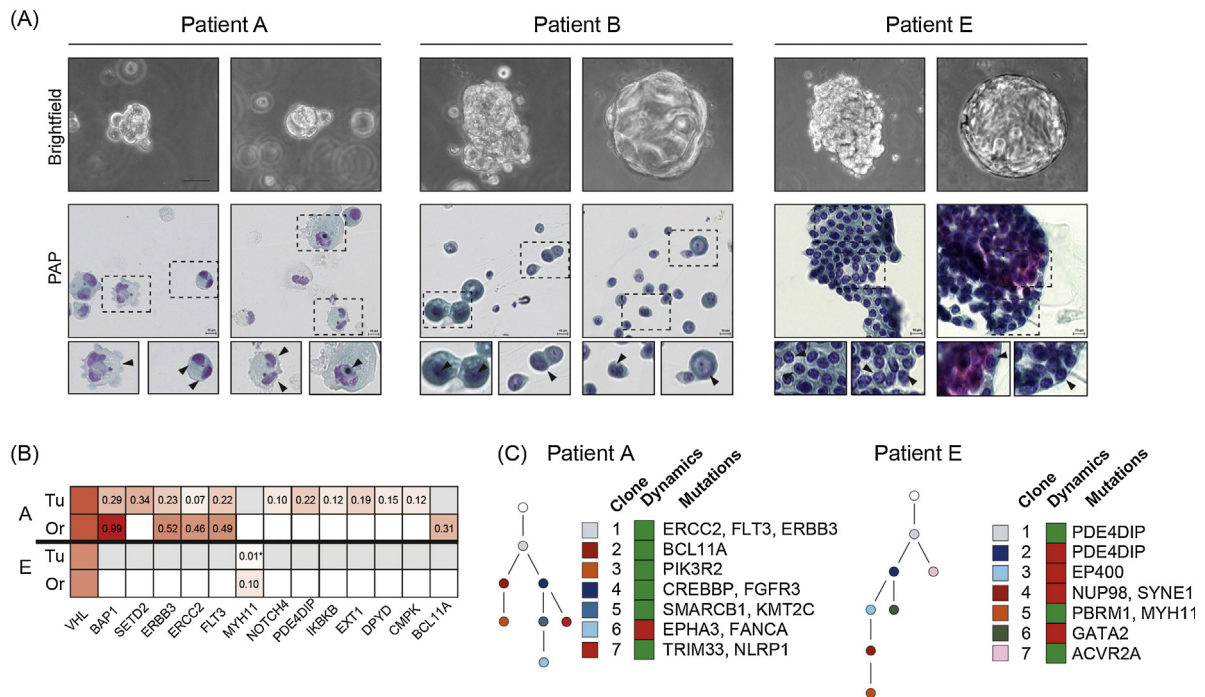
Fig. 5 – Generation and characterization of ccRCC patient-derived three-dimensional (3D) organoid models. (A) Histopathological analysis of tumor organoids generated using Matrigel. Cryopreserved cells from patient A (passage 9), patient B, and patient E (dissociated primary cancer cells) were used for organoid formation. Brightfield images (20× objective) of tumor organoids; scale bar denotes 30 μm. Pap-stained smears (40× objective) of tumor organoids showing characteristic features of malignancy (magnified in insets: multiple pleomorphic nuclei, large nucleoli). (B) High-confidence, nonsilent somatic variants identified by NGS in DNA extracted from primary tumor and organoids. VAFs are indicated and correspond to the color scale. VAFs marked with an asterisk were identified by manual inspection only as they failed to be reported during variant calling. (C) Plots display clonal structures of 3D PDC organoids relative to the tumor samples of patients A and E. Mutation clusters and dynamics were inferred by PhyloWGS from bulk population-level targeted sequencing data. Mutation tree reconstruction allowed the assessment of mutational histories and relationships between subclones. Coding variants defining a new node are shown, and clusters that overlapped between 2D and 3D cell models are color coded correspondingly (refer to Fig. 4A and 4E). Clonal dynamics during organoid derivation and propagation are indicated by green and red squares, respectively, which specify whether the prevalence of subclones increases or decreases in the organoid models relative to the original tumor sample. ccRCC = clear cell renal cell carcinoma; NGS = next-generation sequencing; PDC = patient-derived cell; VAF = variant allele frequency.

contrary, were evenly sized and easily adaptable to multi-well drug testing. Overall, monolayer cultures, microtissues, and organoids derived from the same ccRCC displayed similar drug sensitivities. Three-dimensional models showed greater responses to everolimus, and particularly microtissues were more susceptible to the drug effect at lower concentrations, indicating that the choice of cell culture model may influence the efficiency of drug discovery. In the present setting, matched normal PDCs were not obtained and thus no control was available to assess the toxicity of the targeted agents. Taken together, our results show that 3D cell culture technologies can be applied to PDCs from ccRCCs, and this may enable important advances in drug discovery and fundamental biology.

4. Discussion

Modeling of renal cancer *in vitro* forms the basis of translational research, and is crucial to advance the understanding and treatment options for the disease. Immortalized RCC cell lines have served as the workhorse for preclinical studies for decades, but it is increasingly evident that they often fail to recapitulate the clinical and molecular heterogeneity of human renal tumors [10–12]. To achieve a more adequate

representation of ccRCC *in vitro*, we successfully generated patient-derived 2D and 3D cell models from surgical specimens and confirmed that they retain features of the corresponding patient tumors, such as histology, biomarker expression, cancer driver, and CNAs. Our comprehensive genetic and clonality analyses provided insights into the capability of modeling patient-specific mutational profiles and subclonal diversity of ccRCCs in different cell culture systems [4,6,8]. We present evidence that 2D and 3D PDC culture models capture ccRCC inter- and intratumor heterogeneity, and experimentally confirm that different cell culture techniques influence clonal dynamics *in vitro*. We perceive that the observed differences in genetic alterations between tumor and corresponding PDC models could stem from the selection of subclonal populations occurring *in vitro*, but could partly also result from heterogeneity of the original tumor and consequently from sampling discrepancies. The former scenario is supported by the finding that several mutations have higher variant allele frequencies subsequent to sequential passaging of PDCs. It is likely that these confer a growth advantage *in vitro* and may therefore be more readily detected in PDC cultures. Genetic stability of PDC models was reflected by the almost complete absence of de novo mutations emerging during cell cultivation. Notably, a recent

study highlighting the genetic and clonal evolution of ccRCC suggested at least seven distinct evolutionary subtypes with different clinical prognoses [8]. It is an interesting possibility that PDC cultures can represent the evolutionary potential of ccRCC subsets *in vitro*, or may even offer insights into aggressiveness and treatment susceptibility of the tumors *in vivo*. Indeed, the tumor as well as the cell models derived from patient A seemed to resemble the BAP1-driven evolutionary subtype with a less complex subclonal architecture, elevated chromosomal aberrations, and rapid dissemination to the adrenal gland. The ccRCC of patient D seemed to harbor the largest clonal complexity. Moreover, we detected a clonal mutation in PBRM1 concomitant with chromosomal aberrations, particularly of chromosome 9. Together with the reported absence of metastasis during follow-up of the patient, this case is likely associated with the PBRM1-CNA evolutionary subtype [8]. The PDC cultures that we derived largely retained the characterizing molecular features defining ccRCC evolutionary subtypes during serial passaging and consequently represent attractive tools to study the role of subclones in invasion, metastasis, or therapy resistance. Interestingly, a complementary proof-of-concept study recently indicated the impact of spatial tumor heterogeneity on drug response patterns by establishing PDC cultures from different tumor regions and highlighting their distinct drug response profiles [27]. While truncal driver mutations inherited by all cancer cells could be exploited to find common drug efficacies, PDC models provide the prerequisite to investigate drug response profiles specific to subsets of patients. In fact, proof-of-principle drug sensitivity profiling on multiple PDC models described here revealed variable response patterns that were not predictable by either the genetic analysis of the original ccRCCs or the interrogation of drug effects in commercially available RCC cell lines. State-of-the-art 3D patient-derived models such as organoids and microtissues represent complementary cell culture tools that can potentially mirror additional biological aspects such as spatial interactions of the human tumor [28]. Even though statistically not representative, we showed that for a selected case, 2D and 3D cell models displayed comparable drug sensitivities to clinically approved ccRCC therapeutics. Given that both clonal composition and responses to anticancer agents are likely influenced by cell culture system and culturing conditions [13,29,30], it will be interesting to investigate how the use of different technologies affect subclonal dynamics *in vitro* and whether this is reflective of tumor evolution *in vivo*.

5. Conclusions

Although the implications of several of the findings presented here need further investigation, our data provide the first confirmation that patient-derived *in vitro* models not only capture ccRCC histology and driver genetic alterations, but also reflect patient inter- and intratumor heterogeneity. The presented methods and results will further advance the generation of essential next-generation cell culture available for cancer research and the rational design of targeted treatment strategies for ccRCC.

Appendix A. Supplementary data

Supplementary material related to this article can be found, in the online version, at doi:https://doi.org/10.1016/j.euf.2019.06.009.

References

[1] Fisher R, Gore M, Larkin J. Current and future systemic treatments for renal cell carcinoma. Semin Cancer Biol 2013;23:38–45.

[2] Network TCGAR. Comprehensive molecular characterization of clear cell renal cell carcinoma. Nature 2013;499:43–9.

[3] Frew IJ, Moch H. A clearer view of the molecular complexity of clear cell renal cell carcinoma. Annu Rev Pathol 2015;10:263–89.

[4] Mitchell TJ, Turajlic S, Rowan A, et al. Timing the landmark events in the evolution of clear cell renal cell cancer: TRACERx renal. Cell 2018;173, 611–23.e17.

[5] Hsieh JJ, Purdue MP, Signoretti S, et al. Renal cell carcinoma. Nat Rev Dis Primers 2017;3:17009.

[6] Gerlinger M, Rowan AJ, Horswell S, et al. Intratumor heterogeneity and branched evolution revealed by multiregion sequencing. N Engl J Med 2012;366:883–92.

[7] Gerstung M, Beisel C, Rechsteiner M, et al. Reliable detection of subclonal single-nucleotide variants in tumour cell populations. Nat Commun 2012;3:811.

[8] Turajlic S, Xu H, Litchfield K, et al. Deterministic evolutionary trajectories influence primary tumor growth: TRACERx renal. Cell 2018;173, 595–610.e11.

[9] Bedard PL, Hansen AR, Ratain MJ, Siu LL. Tumour heterogeneity in the clinic. Nature 2013;501:355–64.

[10] Beroukhim R, Brunet JP, Di Napoli A, et al. Patterns of gene expression and copy-number alterations in von-Hippel Lindau disease-associated and sporadic clear cell carcinoma of the kidney. Cancer Res 2009;69:4674–81.

[11] Beleut M, Zimmermann P, Baudis M, et al. Integrative genome-wide expression profiling identifies three distinct molecular subgroups of renal cell carcinoma with different patient outcome. BMC Cancer 2012;12:310.

[12] Horvath P, Aulner N, Bickle M, et al. Screening out irrelevant cell-based models of disease. Nat Rev Drug Discov 2016;15:751–69.

[13] Ben-David U, Siranosian B, Ha G, et al. Genetic and transcriptional evolution alters cancer cell line drug response. Nature 2018;560:325–30.

[14] Corro C, Hejhal T, Poyet C, et al. Detecting circulating tumor DNA in renal cancer: an open challenge. Exp Mol Pathol 2017;102:255–61.

[15] Escudier B, Porta C, Schmidinger M, et al. Renal cell carcinoma: ESMO clinical practice guidelines for diagnosis, treatment and follow-up. Ann Oncol 2014;25(Suppl 3):iii49–56.

[16] Escudier B, Lougheed JC, Albiges L. Cabozantinib for the treatment of renal cell carcinoma. Expert Opin Pharmacother 2016;17:2499–504.

[17] Wallis CJD, Klaassen Z, Bhindi B, et al. First-line systemic therapy for metastatic renal cell carcinoma: a systematic review and network meta-analysis. Eur Urol 2018;74:309–21.

[18] Wong SQ, Li J, AY-C Tan, et al. Sequence artefacts in a prospective series of formalin-fixed tumours tested for mutations in hotspot regions by massively parallel sequencing. BMC Med Genom 2014;7:23.

[19] Deshwar AG, Vembu S, Yung CK, Jang GH, Stein L, Morris Q. PhyloWGS: reconstructing subclonal composition and evolution from whole-genome sequencing of tumors. Genome Biol 2015;16:35.

[20] Turajlic S, Xu H, Litchfield K, et al. Tracking cancer evolution reveals constrained routes to metastases: TRACERx renal. Cell 2018;173, 581–94.e12.

[21] Clevers H. Modeling development and disease with organoids. Cell 2016;165:1586–97.

[22] Thoma CR, Zimmermann M, Agarkova I, Kelm JM, Krek W. 3D cell culture systems modeling tumor growth determinants in cancer target discovery. Adv Drug Deliv Rev 2014;69–70:29–41.

[23] Pauli C, Hopkins BD, Prandi D, et al. Personalized in vitro and in vivo cancer models to guide precision medicine. Cancer Discov 2017;7:462–77.

[24] Sachs N, de Ligt J, Kopper O, et al. A living biobank of breast cancer organoids captures disease heterogeneity. Cell 2018;172, 373–86.e10.

[25] Thompson JM, Nguyen QH, Singh M, et al. Rho-associated kinase 1 inhibition is synthetically lethal with von Hippel-Lindau deficiency in clear cell renal cell carcinoma. Oncogene 2016;36:1080.

[26] Fischer AH, Zhao C, Li QK, et al. The cytologic criteria of malignancy. J Cell Biochem 2010;110:795–811.

[27] Saeed K, Ojamies P, Pellinen T, et al. Clonal heterogeneity influences drug responsiveness in renal cancer assessed by ex vivo drug testing of multiple patient-derived cancer cells. Int J Cancer 2019;144:1356–66.

[28] Drost J, Clevers H. Organoids in cancer research. Nat Rev Cancer 2018;18:407–18.

[29] Pickl M, Ries CH. Comparison of 3D and 2D tumor models reveals enhanced HER2 activation in 3D associated with an increased response to trastuzumab. Oncogene 2009;28:461–8.

[30] Carragher N, Piccinini F, Tesei A, Trask Jr OJ, Bickle M, Horvath P. Concerns, challenges and promises of high-content analysis of 3D cellular models. Nat Rev Drug Discov 2018;17:606.